



## RESEARCH ARTICLE

# Lie group based nonlinear state errors for MEMS-IMU/GNSS/magnetometer integrated navigation

Jiarui Cui,  Maosong Wang, \* Wenqi Wu,  and Xiaofeng He

College of Intelligence Science and Technology, National University of Defense Technology, Changsha, Hunan, P.R. China.

\*Corresponding author. E-mail: [wangmaosong12@hotmail.com](mailto:wangmaosong12@hotmail.com)

**Received:** 8 June 2020; **Accepted:** 10 February 2021; **First published online:** 11 March 2021

**Keywords:** integrated navigation, nonlinear state error, LG-EKF, MIMU/GNSS/magnetometer integration

## Abstract

In the integrated navigation system using extended Kalman filter (EKF), the state error conventionally uses linear approximation to tackle the commonly nonlinear problem. However, this error definition can diverge the filter in some adverse situations due to significant distortion of the linear approximation. By contrast, the nonlinear state error defined in the Lie group satisfies the autonomous equation, which thus has distinctively better convergence property. This work proposes a novel strapdown inertial navigation system (SINS) nonlinear state error defined in the Lie group and derives the SINS equations of the Lie group EKF (LG-EKF) for the MIMU/GNSS/magnetometer integrated navigation system. The corresponding measurement equations are also derived. A land vehicle field test has been conducted to evaluate the performance of EKF, ST-EKF (state transformation extended Kalman filter) and LG-EKF, which verifies LG-EKF's superior estimation accuracy of the heading angle as well as the other two horizontal angles (pitch and roll). The LG-EKF proposed in this paper is unlimited in the choice of sensors, which means it can be applied with both high-end and low-end inertial sensors.

## 1. Introduction

The recent development of micro-electro-mechanical system (MEMS) technologies has made MEMS inertial measurement units (IMU) available at a lower price and considerable precision, making MEMS-IMU an ideal inertial sensor in many industrial and military navigation appliances (Jang and Liccardo, 2007; Leclerc, 2007; Ravish et al., 2013). With the global navigation satellite system (GNSS) signal thus aided, land and aerial vehicles can achieve high-precision integrated navigation. However, due to the low heading damping in strapdown inertial navigation system (SINS)/GNSS integrated navigation, additional heading information is needed to improve the precision, such as magnetometer (Cui et al., 2019) and polarised light (Liang et al., 2020). The magnetometer is more common in navigation applications and its calibration method has been investigated extensively (Wu et al., 2018; Wu, 2019; Xiang et al., 2019). Therefore, a well-calibrated magnetometer-aided attitude estimation system has become a favoured supplement in low-cost applications (Wu et al., 2016; Miao et al., 2014).

Extended Kalman Filter (EKF) is the most popular estimator in SINS; it utilises the Riccati equation to achieve adaptive gain tuning to handle the time-varying nature of the linearised error equation (Sebesta and Boizot, 2014; Brossard et al., 2019). The conventional EKF state error is usually the first-order linearisation of the real nonlinear system, which requires state error to be sufficiently small. However, this strict condition relies greatly on the actual estimated states, which cannot always be met when the navigation system states have a large deviation from real initial values, possibly causing the covariance inconsistency problem and even diverging the Kalman filter (Hartley et al., 2020). For instance, the paper Robert and Perrot (2017) illustrated a case where vibration of the vehicle mistakenly

causes the estimated covariance of the unobservable error state to undergo continuous reduction. To solve the covariance inconsistency problem, Huang et al. (2010) used the observability-constrained EKF (OC-EKF) to optimise the linearisation points and therefore minimise the linearisation error. Schmidt (1966) proposed the Schmidt-Kalman filter (S-KF) setting the unobservable state covariance to zero.

Nevertheless, these methodologies do not change the nature of the nonlinearity problem of state errors due to the linear approximation. Wang et al. (2018) proposed the state transformation EKF (ST-EKF), which used a new velocity nonlinear error state, and showed robustness and accuracy improvement in high-precision navigation applications significantly. The invariant Kalman filter (Barrau and Bonnabel, 2017a; 2020) which utilised the theory of symmetry preserving observers demonstrated that, for the left-invariant system on the Lie group, the nonlinear observer could be designed to make the right-invariant (or left-invariant) error state obey the autonomous equation. This nonlinear observer has a rare property of trajectory independence, which means that even if the navigation state undergoes nonlinear changes, the error state evolution still follows a linear differential equation. The invariant Kalman filter theory has been widely used and provided performance improvement in many navigation engineering cases (Barrau and Bonnabel, 2017b; Brossard et al., 2018; Hartley et al., 2020).

The contributions and organisation of this paper are as follows. In section 2, the SINS equations with regard to the Earth-centred inertial (ECI) frame resolving in Earth-centred Earth-fixed (ECEF) frame are derived. And then in section 3, the proof that the proposed nonlinear state errors based on the matrix Lie group methodology satisfy trajectory independent error propagation property is given. The common frame definitions of SINS state errors are then presented in section 4. The detailed system equation of LG-EKF is also derived. In section 5, the new measurement equation for SINS/GNSS/magnetometer integration is developed. Section 6 reports a land vehicle field test that was conducted to compare the performance of EKF, ST-EKF and LG-EKF, in which LG-EKF achieved more accurate estimation of all the three attitude angles. The LG-EKF proposed in this paper can be applied in integrated navigation systems no matter whether they are based on high-end or low-end inertial sensors.

## 2. SINS navigation differential equation in ECEF frame

The new full state SINS differential equations are derived first to obtain the SINS state error differential equations subsequently. The coordinate frames are declared as follows.

*i* frame: ECI frame.

*e* frame: ECEF frame.

*n* frame: Local navigation frame. Its origin is the object described by the navigation solution. Here it is the North-East-Down frame.

*b* frame: Body frame. This is commonly the IMU frame, which comprises the origin and orientation of the object described by the navigation solution.

$C_b^e$  represents the direction cosine matrix transforming *b* frame to *e* frame;  $v_{ib}^e$  is the body velocity with regard to the *i* frame resolving in *e* frame;  $r_{ib}^e$  is the position vector pointing from *i* frame's origin to *b* frame's origin projected in *e* frame. Other symbols also follow similar naming rules.

The time derivative of  $C_b^e$  can be derived

$$\dot{C}_b^e = C_b^e(\omega_{ib}^b \wedge) - (\omega_{ie}^e \wedge)C_b^e \quad (1)$$

and the time derivative of  $v_{ib}^i$  is also expressed as

$$\dot{v}_{ib}^i = C_b^i f^b + g_{ib}^i \quad (2)$$

where  $f^b$  is the specific force;  $g_{ib}^i$  is the local gravitational acceleration projected in *i* frame.

From Equation (2) the time derivative of  $v_{ib}^e$  can be derived

$$\dot{v}_{ib}^e = \frac{d}{dt}(C_i^e v_{ib}^i) = -(\omega_{ie}^e \wedge) v_{ib}^e + C_i^e C_b^i f^b + C_i^e g_{ib}^i = C_b^e f^b - (\omega_{ie}^e \wedge) v_{ib}^e + g_{ib}^e \tag{3}$$

where the differential equation  $\dot{C}_e^i = C_e^i(\omega_{ie}^e \wedge)$  is used;  $g_{ib}^e$  is the local gravitational acceleration projected in  $e$  frame.

The time derivative of the  $r_{ib}^e$  can be derived as

$$\dot{r}_{ib}^e = \frac{d}{dt}(C_i^e r_{ib}^i) = -(\omega_{ie}^e \wedge) C_i^e r_{ib}^i + C_i^e \dot{r}_{ib}^i = -(\omega_{ie}^e \wedge) r_{ib}^e + v_{ib}^e \tag{4}$$

Equations (1), (3) and (4) form the full state SINS navigation differential equations, which build up the basis of the derivation of the nonlinear state error equations in section 4.

### 3. Proof of the invariance property of new SINS nonlinear states

This section gives the detailed proof that the navigation states defined in Equations (1), (3) and (4) satisfy the autonomous error equation in Barrau and Bonnabel (2017a), which means that they have invariance property. For more details of the invariance property, refer to Barrau and Bonnabel (2017a).

Define the dynamic system differential equation as

$$\frac{d}{dt}\chi = f_{u_t}(\chi) \tag{5}$$

where the state  $\chi$  lives in the Lie group and  $u_t$  represents a certain input. Define the right-invariant error as  $\eta^R = \chi \tilde{\chi}^{-1}$ , where  $\tilde{\chi}$  is the estimated state. According to Theorem 1 in Barrau and Bonnabel (2017a), if  $f_{u_t}(\chi)$  satisfies Equation (6), then  $\eta^R$  is said to have a state trajectory independent property.

$$f_{u_t}(\chi_A \chi_B) = f_{u_t}(\chi_A) \chi_B + \chi_A f_{u_t}(\chi_B) - \chi_A f_{u_t}(\mathbf{I}_d) \chi_B \tag{6}$$

where the two states  $\chi_A$  and  $\chi_B$  live in the Lie group and  $\mathbf{I}_d$  is the identity matrix.

Moreover, if  $\eta^R$  is state trajectory independent, the Equation (7) is satisfied as well.

$$\frac{d}{dt}\eta^R = g_{u_t}(\eta^R) = f_{u_t}(\eta^R) - \eta^R f_{u_t}(\mathbf{I}_d) \tag{7}$$

The property of Equation (6) is proved first. The system state  $\chi$  and its corresponding inverse  $\chi^{-1}$  are defined as

$$\chi = \begin{bmatrix} C_b^e & v_{ib}^e & r_{ib}^e \\ \mathbf{0}_{1 \times 3} & 1 & 0 \\ \mathbf{0}_{1 \times 3} & 0 & 1 \end{bmatrix}, \quad \chi^{-1} = \begin{bmatrix} C_b^e & -v_{ib}^e & -r_{ib}^e \\ \mathbf{0}_{1 \times 3} & 1 & 0 \\ \mathbf{0}_{1 \times 3} & 0 & 1 \end{bmatrix} \tag{8}$$

Then, the differential of  $\chi$  can be derived

$$\begin{aligned} \frac{d}{dt}\chi = f_{u_t}(\chi) &= \frac{d}{dt} \begin{bmatrix} C_b^e & v_{ib}^e & r_{ib}^e \\ \mathbf{0}_{1 \times 3} & 1 & 0 \\ \mathbf{0}_{1 \times 3} & 0 & 1 \end{bmatrix} = \begin{bmatrix} \dot{C}_b^e & \dot{v}_{ib}^e & \dot{r}_{ib}^e \\ \mathbf{0}_{1 \times 3} & 0 & 0 \\ \mathbf{0}_{1 \times 3} & 0 & 0 \end{bmatrix} = \chi W_1 + W_2 \chi \\ &= \begin{bmatrix} C_b^e & v_{ib}^e & r_{ib}^e \\ \mathbf{0}_{1 \times 3} & 1 & 0 \\ \mathbf{0}_{1 \times 3} & 0 & 1 \end{bmatrix} \begin{bmatrix} (\omega_{ib}^b \wedge) f^b & \mathbf{0}_{3 \times 1} \\ \mathbf{0}_{1 \times 3} & 0 & 0 \\ \mathbf{0}_{1 \times 3} & 0 & 0 \end{bmatrix} + \begin{bmatrix} -(\omega_{ie}^e \wedge) g_{ib}^e & v_{ib}^e \\ \mathbf{0}_{1 \times 3} & 0 & 0 \\ \mathbf{0}_{1 \times 3} & 0 & 0 \end{bmatrix} \begin{bmatrix} C_b^e & v_{ib}^e & r_{ib}^e \\ \mathbf{0}_{1 \times 3} & 1 & 0 \\ \mathbf{0}_{1 \times 3} & 0 & 1 \end{bmatrix} \end{aligned} \tag{9}$$

where

$$W_1 = \begin{bmatrix} (\omega_{ib}^b \wedge) f^b & \mathbf{0}_{3 \times 1} \\ \mathbf{0}_{1 \times 3} & 0 & 0 \\ \mathbf{0}_{1 \times 3} & 0 & 0 \end{bmatrix}, \quad W_2 = \begin{bmatrix} -(\omega_{ie}^e \wedge) \mathbf{g}_{ib}^e & \mathbf{v}_{ib}^e \\ \mathbf{0}_{1 \times 3} & 0 & 0 \\ \mathbf{0}_{1 \times 3} & 0 & 0 \end{bmatrix} \tag{10}$$

Let

$$\mathcal{X}_A = \begin{bmatrix} C_{bA}^e & \mathbf{v}_{ibA}^e & \mathbf{r}_{ibA}^e \\ \mathbf{0}_{1 \times 3} & 1 & 0 \\ \mathbf{0}_{1 \times 3} & 0 & 1 \end{bmatrix}, \quad \mathcal{X}_B = \begin{bmatrix} C_{bB}^e & \mathbf{v}_{ibB}^e & \mathbf{r}_{ibB}^e \\ \mathbf{0}_{1 \times 3} & 1 & 0 \\ \mathbf{0}_{1 \times 3} & 0 & 1 \end{bmatrix} \tag{11}$$

therefore

$$\mathcal{X}_A \mathcal{X}_B = \begin{bmatrix} C_{bA}^e & \mathbf{v}_{ibA}^e & \mathbf{r}_{ibA}^e \\ \mathbf{0}_{1 \times 3} & 1 & 0 \\ \mathbf{0}_{1 \times 3} & 0 & 1 \end{bmatrix} \begin{bmatrix} C_{bB}^e & \mathbf{v}_{ibB}^e & \mathbf{r}_{ibB}^e \\ \mathbf{0}_{1 \times 3} & 1 & 0 \\ \mathbf{0}_{1 \times 3} & 0 & 1 \end{bmatrix} = \begin{bmatrix} C_{bA}^e C_{bB}^e & \mathbf{v}_{ibA}^e + C_{bA}^e \mathbf{v}_{ibB}^e & \mathbf{r}_{ibA}^e + C_{bA}^e \mathbf{r}_{ibB}^e \\ \mathbf{0}_{1 \times 3} & 1 & 0 \\ \mathbf{0}_{1 \times 3} & 0 & 1 \end{bmatrix} \tag{12}$$

According to Equation (9), we have  $f_{u_t}(\mathbf{I}_d) = W_1 + W_2$  and  $f_{u_t}(\mathcal{X}_A \mathcal{X}_B) = \mathcal{X}_A \mathcal{X}_B W_1 + W_2 \mathcal{X}_A \mathcal{X}_B$ . Therefore, the right side of Equation (6) can be written as

$$\begin{aligned} & f_{u_t}(\mathcal{X}_A) \mathcal{X}_B + \mathcal{X}_A f_{u_t}(\mathcal{X}_B) - \mathcal{X}_A f_{u_t}(\mathbf{I}_d) \mathcal{X}_B \\ &= \mathcal{X}_A W_1 \mathcal{X}_B + W_2 \mathcal{X}_A \mathcal{X}_B + \mathcal{X}_A \mathcal{X}_B W_1 + \mathcal{X}_A W_2 \mathcal{X}_B - \mathcal{X}_A (W_1 + W_2) \mathcal{X}_B \\ &= \mathcal{X}_A \mathcal{X}_B W_1 + W_2 \mathcal{X}_A \mathcal{X}_B = f_{u_t}(\mathcal{X}_A \mathcal{X}_B) \end{aligned} \tag{13}$$

Here we have proved that the navigation states defined in Equations (1), (3) and (4) satisfy the property of Equation (6). The right-invariant error  $\eta^R$  satisfies the property of Equation (7) is also proved next.

From Equation (8), we have

$$\eta^R = \mathcal{X} \tilde{\chi}^{-1} = \begin{bmatrix} C_b^e & \mathbf{v}_{ib}^e & \mathbf{r}_{ib}^e \\ \mathbf{0}_{1 \times 3} & 1 & 0 \\ \mathbf{0}_{1 \times 3} & 0 & 1 \end{bmatrix} \begin{bmatrix} \tilde{C}_e^b & -\tilde{\mathbf{v}}_{ib}^b & -\tilde{\mathbf{r}}_{ib}^b \\ \mathbf{0}_{1 \times 3} & 1 & 0 \\ \mathbf{0}_{1 \times 3} & 0 & 1 \end{bmatrix} = \begin{bmatrix} C_b^e \tilde{C}_e^b & \mathbf{v}_{ib}^e - C_b^e \tilde{\mathbf{v}}_{ib}^b & \mathbf{r}_{ib}^e - C_b^e \tilde{\mathbf{r}}_{ib}^b \\ \mathbf{0}_{1 \times 3} & 1 & 0 \\ \mathbf{0}_{1 \times 3} & 0 & 1 \end{bmatrix} \tag{14}$$

Substitute Equation (14) into (7),

$$\begin{aligned} \frac{d}{dt} \eta^R &= g_{u_t}(\eta^R) = f_{u_t}(\eta^R) - \eta^R f_{u_t}(\mathbf{I}_d) = \eta^R W_1 + W_2 \eta^R - \eta^R (W_1 + W_2) \\ &= W_2 \eta^R - \eta^R W_2 = \begin{bmatrix} -(\omega_{ie}^e \wedge) \mathbf{g}_{ib}^e & \mathbf{v}_{ib}^e \\ \mathbf{0}_{1 \times 3} & 0 & 0 \\ \mathbf{0}_{1 \times 3} & 0 & 0 \end{bmatrix} \eta^R - \eta^R \begin{bmatrix} -(\omega_{ie}^e \wedge) \mathbf{g}_{ib}^e & \mathbf{v}_{ib}^e \\ \mathbf{0}_{1 \times 3} & 0 & 0 \\ \mathbf{0}_{1 \times 3} & 0 & 0 \end{bmatrix} \end{aligned} \tag{15}$$

Thus, the property in Equation (7) has been verified. The proofs above have proved that the navigation states defined in Equations (1), (3) and (4) possess the rare trajectory independent error propagation property, which means that even if the change of the state error is nonlinear, its propagation remains linear. In the next section, the differential equations of the SINS nonlinear state errors are derived in detail.

#### 4. The differential equations of the SINS nonlinear state error

The new SINS nonlinear state errors related to the attitude, velocity and position can be obtained from the right-invariant errors in Equation (14).

Define the new SINS state errors

$$\begin{aligned}
 \mathbf{C}_b^e \tilde{\mathbf{C}}_e^b &= \exp(\boldsymbol{\phi}^e \wedge) \\
 \mathbf{J}\boldsymbol{\rho}_v^e &= \mathbf{v}_{ib}^e - \mathbf{C}_b^e \tilde{\mathbf{v}}_{ib}^b = (\mathbf{v}_{ib}^e - \tilde{\mathbf{v}}_{ib}^e) + (\mathbf{I} - \mathbf{C}_b^e \tilde{\mathbf{C}}_e^b) \tilde{\mathbf{v}}_{ib}^e = -\delta \mathbf{v}_{ib}^e + (\mathbf{I} - \exp(\boldsymbol{\phi}^e \wedge)) \tilde{\mathbf{v}}_{ib}^e \\
 \mathbf{J}\boldsymbol{\rho}_r^e &= \mathbf{r}_{ib}^e - \mathbf{C}_b^e \tilde{\mathbf{r}}_{ib}^b = (\mathbf{r}_{ib}^e - \tilde{\mathbf{r}}_{ib}^e) + (\mathbf{I} - \mathbf{C}_b^e \tilde{\mathbf{C}}_e^b) \tilde{\mathbf{r}}_{ib}^e = -\delta \mathbf{r}_{ib}^e + (\mathbf{I} - \exp(\boldsymbol{\phi}^e \wedge)) \tilde{\mathbf{r}}_{ib}^e
 \end{aligned} \tag{16}$$

where  $\boldsymbol{\phi}^e$  is the misalignment angle vector,  $\mathbf{J}\boldsymbol{\rho}_v^e$  and  $\mathbf{J}\boldsymbol{\rho}_r^e$  denote the new nonlinear velocity error vector and position error vector, respectively;  $\exp(\cdot)$  is the matrix exponential. Compared with the linear state errors, which are the direct difference of the vectors in the computational coordinate frame and the real coordinate frame, the new nonlinear state errors are defined in the common coordinate frame (Andrieu and Crassidis, 2015). More specifically, the new nonlinear state errors consider both the magnitude difference and the direction difference of two vectors, which can lead to provable convergence properties of the Kalman filter.

Rewrite the right-invariant error  $\boldsymbol{\eta}^R$  in Equation (14)

$$\boldsymbol{\eta}^R = \begin{bmatrix} \exp(\boldsymbol{\phi}^e \wedge) & \mathbf{J}\boldsymbol{\rho}_v^e & \mathbf{J}\boldsymbol{\rho}_r^e \\ \mathbf{0}_{1 \times 3} & 1 & 0 \\ \mathbf{0}_{1 \times 3} & 0 & 1 \end{bmatrix} \tag{17}$$

In order to establish the system equation of the Kalman filter, the differential equations of  $\boldsymbol{\phi}^e$ ,  $\mathbf{J}\boldsymbol{\rho}_v^e$  and  $\mathbf{J}\boldsymbol{\rho}_r^e$  must be derived.

Assume that the gyroscope and accelerometer measurements contain noise and can be expressed as

$$\begin{aligned}
 \tilde{\boldsymbol{\omega}}_{ib}^b &= \boldsymbol{\omega}_{ib}^b + \delta \boldsymbol{\omega}_{ib}^b = \boldsymbol{\omega}_{ib}^b + \boldsymbol{\varepsilon}^b + \mathbf{w}_g \\
 \tilde{\mathbf{f}}^b &= \mathbf{f}^b + \delta \mathbf{f}^b = \mathbf{f}^b + \nabla^b + \mathbf{w}_a
 \end{aligned} \tag{18}$$

where  $\mathbf{w}_g$  is the white noise vector of the gyroscopes and  $\mathbf{w}_a$  is the white noise vector of the accelerometers;  $\boldsymbol{\varepsilon}^b$  is the bias vector of gyroscopes and  $\nabla^b$  is the bias vector of accelerometers, which are constant values with differential equations

$$\dot{\boldsymbol{\varepsilon}}^b = \mathbf{0}, \quad \dot{\nabla}^b = \mathbf{0} \tag{19}$$

The differential equation of the misalignment angle  $\boldsymbol{\phi}^e$  is derived as follows. First, the derivative of  $\mathbf{C}_b^e \tilde{\mathbf{C}}_e^b$  can be derived as

$$\begin{aligned}
 \frac{d}{dt}(\mathbf{C}_b^e \tilde{\mathbf{C}}_e^b) &= \dot{\mathbf{C}}_b^e \tilde{\mathbf{C}}_e^b + \mathbf{C}_b^e \dot{\tilde{\mathbf{C}}}_e^b \\
 &= \mathbf{C}_b^e \tilde{\mathbf{C}}_e^b (\boldsymbol{\omega}_{ie}^e \wedge) - (\boldsymbol{\omega}_{ie}^e \wedge) \mathbf{C}_b^e \tilde{\mathbf{C}}_e^b - \mathbf{C}_b^e ((\boldsymbol{\varepsilon}^b + \mathbf{w}_g) \wedge) \mathbf{C}_b^e
 \end{aligned} \tag{20}$$

The first-order approximation of  $\mathbf{C}_b^e \tilde{\mathbf{C}}_e^b$  is

$$\mathbf{C}_b^e \tilde{\mathbf{C}}_e^b = \exp(\boldsymbol{\phi}^e \wedge) \approx \mathbf{I} + \boldsymbol{\phi}^e \wedge \tag{21}$$

Substitute Equation (21) into (20), then the derivative of  $\boldsymbol{\phi}^e$  can be expressed as

$$\frac{d}{dt}(\boldsymbol{\phi}^e) = -\boldsymbol{\omega}_{ie}^e \wedge \boldsymbol{\phi}^e - \mathbf{C}_b^e \boldsymbol{\varepsilon}^b - \mathbf{C}_b^e \mathbf{w}_g \tag{22}$$

The differential equation of the new velocity error  $\mathbf{J}\rho_v^e$  is derived as

$$\begin{aligned} \frac{d}{dt}(\mathbf{J}\rho_v^e) &= \frac{d}{dt}((v_{ib}^e - \tilde{v}_{ib}^e) + (\mathbf{I} - \mathbf{C}_b^e \tilde{\mathbf{C}}_e^b) \tilde{v}_{ib}^e) = \frac{d}{dt}(v_{ib}^e - \mathbf{C}_b^e \tilde{\mathbf{C}}_e^b \tilde{v}_{ib}^e) \\ &= \left[ (\mathbf{g}_{ib}^e \wedge) + \frac{\mu}{|\mathbf{r}_{ib}^e|^3} (\mathbf{r}_{ib}^e \wedge) \right] \boldsymbol{\phi}^e - (\omega_{ie}^e \wedge) \mathbf{J}\rho_v^e - \frac{\mu}{|\mathbf{r}_{ib}^e|^3} (\mathbf{J}\rho_r^e) \\ &\quad - (\tilde{v}_{ib}^e \wedge) \mathbf{C}_b^e (\boldsymbol{\varepsilon}^b + \mathbf{w}_g) - \mathbf{C}_b^e (\nabla^b + \mathbf{w}_a) \end{aligned} \tag{23}$$

where  $\delta \mathbf{g}_{ib}^e \approx -\frac{\mu}{|\mathbf{r}_{ib}^e|^3} \delta \mathbf{r}_{ib}^e \approx \frac{\mu}{|\mathbf{r}_{ib}^e|^3} (\mathbf{J}\rho_r^e - \mathbf{r}_{ib}^e \wedge \boldsymbol{\phi}^e)$  is used and  $\mu$  is defined in Groves (2013).

The differential equation of the new position error  $\mathbf{J}\rho_r^e$  is derived as

$$\begin{aligned} \frac{d}{dt}(\mathbf{J}\rho_r^e) &= \dot{\mathbf{r}}_{ib}^e - \mathbf{C}_b^e \tilde{\mathbf{C}}_e^b \dot{\tilde{\mathbf{r}}}_{ib}^e - \frac{d}{dt}(\mathbf{C}_b^e \tilde{\mathbf{C}}_e^b) \tilde{\mathbf{r}}_{ib}^e \\ &= \mathbf{J}\rho_v^e - (\omega_{ie}^e \wedge) \mathbf{J}\rho_r^e - (\tilde{\mathbf{r}}_{ib}^e \wedge) \mathbf{C}_b^e (\boldsymbol{\varepsilon}^b + \mathbf{w}_g) \end{aligned} \tag{24}$$

According to Equations (19), (22), (23) and (24), all the state error equations of the LG-EKF can be involved as a unified form as Equation (25)

$$\dot{\mathbf{x}}_{LG-EKF} = \mathbf{F}_{LG-EKF} \mathbf{x}_{LG-EKF} + \mathbf{G}_{LG-EKF} \mathbf{w} \tag{25}$$

where  $\mathbf{F}_{LG-EKF}$  is the system matrix,  $\mathbf{x}_{LG-EKF}$  is the state error vector,  $\mathbf{G}_{LG-EKF}$  is the noise shaping matrix. They are detailed as below

$$\mathbf{x}_{LG-EKF} = \left[ (\boldsymbol{\phi}^e)^T \quad (\mathbf{J}\rho_v^e)^T \quad (\mathbf{J}\rho_r^e)^T \quad (\boldsymbol{\varepsilon}^b)^T \quad (\nabla^b)^T \right]^T \tag{26}$$

$$\mathbf{G}_{LG-EKF} = \begin{bmatrix} -\mathbf{C}_b^e & \mathbf{0}_{3 \times 3} \\ -(\mathbf{v}_{ib}^e \wedge) \mathbf{C}_b^e & -\mathbf{C}_b^e \\ -(\tilde{\mathbf{r}}_{ib}^e \wedge) \mathbf{C}_b^e & \mathbf{0}_{3 \times 3} \\ \mathbf{0}_{3 \times 3} & \mathbf{0}_{3 \times 3} \\ \mathbf{0}_{3 \times 3} & \mathbf{0}_{3 \times 3} \end{bmatrix} \tag{27}$$

$$\mathbf{F}_{LG-EKF} = \begin{bmatrix} -(\omega_{ie}^e \wedge) & \mathbf{0}_{3 \times 3} & \mathbf{0}_{3 \times 3} & -\mathbf{C}_b^e & \mathbf{0}_{3 \times 3} \\ \left( \begin{array}{l} (\mathbf{g}_{ib}^e \wedge) \\ + \frac{\mu}{|\mathbf{r}_{ib}^e|^3} (\mathbf{r}_{ib}^e \wedge) \end{array} \right) & -(\omega_{ie}^e \wedge) & -\frac{\mu}{|\mathbf{r}_{ib}^e|^3} & -(\mathbf{v}_{ib}^e \wedge) \mathbf{C}_b^e & -\mathbf{C}_b^e \\ \mathbf{0}_{3 \times 3} & \mathbf{I}_{3 \times 3} & -(\omega_{ie}^e \wedge) & -(\tilde{\mathbf{r}}_{ib}^e \wedge) \mathbf{C}_b^e & \mathbf{0}_{3 \times 3} \\ \mathbf{0}_{3 \times 3} & \mathbf{0}_{3 \times 3} & \mathbf{0}_{3 \times 3} & \mathbf{0}_{3 \times 3} & \mathbf{0}_{3 \times 3} \\ \mathbf{0}_{3 \times 3} & \mathbf{0}_{3 \times 3} & \mathbf{0}_{3 \times 3} & \mathbf{0}_{3 \times 3} & \mathbf{0}_{3 \times 3} \end{bmatrix} \tag{28}$$

Compare the system matrix of LG-EKF in Equation (28) with the system matrix of EKF in Groves (2013); the specific force term has been replaced by the gravitational acceleration term. In engineering applications, the implementation of the conventional EKF requires high-frequency propagation of the system matrix to adequately cover the bandwidth of specific force (Wang et al., 2018, 2019a, 2019b, 2019c). However, in the LG-EKF, high-speed processing of the system matrix has been unnecessary since the gravitational acceleration is more robust for local navigation problems. Therefore, the propagation and updating processes of the Kalman filter can be executed simultaneously at a relatively slower rate, which is more computationally efficient. It should be pointed out that the complete Lie formulae expressions have infinity terms and the process and observation models of the Kalman filter are the

approximation of linearisation which means that the Jacobian of the Lie exponential is not merely the wedge operation (Wu et al., 2020).

The system state error models above are capable of use in almost any SINS based integrated navigation system. The next section develops the velocity and position observation equations, and the heading angle measurement equations for the low-cost MIMU/GNSS/magnetometer integrated navigation system.

### 5. LG-EKF measurement equations for MIMU/GNSS/magnetometer integrated system

The velocity and position measurements are provided by GNSS information. The heading angle measurement is provided by the magnetometer.

The LG-EKF measurement models are a little more complicated than that of the EKF. On the one hand, the navigation parameters  $v_{ib}^e$  and  $r_{ib}^e$  resolved in SINS are with regard to  $i$  frame resolving in  $e$  frame, while the GNSS measurements are generally with regard to  $e$  frame resolving in  $e$  frame. Thus, the following state transformation equations are needed

$$\begin{aligned} \tilde{r}_{ib}^e &= \tilde{r}_{eb}^e, \tilde{r}_{ib}^i = \tilde{r}_{eb}^i, \delta \tilde{r}_{ib}^e = \delta \tilde{r}_{eb}^e, \tilde{v}_{ib}^i = \tilde{v}_{eb}^i + \omega_{ie}^i \times \tilde{r}_{ib}^i, \tilde{v}_{ib}^e = \tilde{v}_{eb}^e + \omega_{ie}^e \times \tilde{r}_{eb}^e \\ \tilde{v}_{eb}^e &= \tilde{v}_{ib}^e - \omega_{ie}^e \times \tilde{r}_{eb}^e, \delta \tilde{v}_{eb}^e = \delta \tilde{v}_{ib}^e - \omega_{ie}^e \times \delta \tilde{r}_{eb}^e \end{aligned} \tag{29}$$

where  $\delta \tilde{r}_{ib}^e$  is the position error with regard to  $i$  frame resolving in  $e$  frame and  $\delta \tilde{r}_{eb}^e$  is the position error with regard to  $e$  frame resolving in  $e$  frame.

The measurement models are described as

$$\begin{aligned} \delta \mathbf{z}_v &= \delta \mathbf{v}_{ib}^e + \mathbf{u}_{v,3 \times 1} = -\mathbf{J} \boldsymbol{\rho}_v^e + [\tilde{\mathbf{v}}_{ib}^e \wedge] \boldsymbol{\phi}^e + \mathbf{u}_{v,3 \times 1} \\ \delta \mathbf{z}_r &= \delta \mathbf{r}_{ib}^e + \mathbf{u}_{r,3 \times 1} = -\mathbf{J} \boldsymbol{\rho}_r^e + [\tilde{\mathbf{r}}_{ib}^e \wedge] \boldsymbol{\phi}^e + \mathbf{u}_{r,3 \times 1} \end{aligned} \tag{30}$$

where  $\delta \mathbf{z}_v$  and  $\delta \mathbf{z}_r$  are the velocity and position errors formed by SINS and GNSS.  $\mathbf{u}_{v,3 \times 1}$  and  $\mathbf{u}_{r,3 \times 1}$  are the corresponding measurement noises, which are generally considered as white noise with certain covariance.

On the other hand, the heading angle  $\psi^n$  provided by the magnetometer is usually projected in the  $n$  frame, whereas the misalignment angle  $\boldsymbol{\phi}^e$  is defined in the  $e$  frame. Therefore, a relationship of  $\psi^n$  with misalignment angle defined in  $e$  frame is needed.

Consider the transformation matrix  $\mathbf{C}_n^e$

$$\mathbf{C}_n^e = \begin{bmatrix} -\sin L \cos \lambda & -\sin L \sin \lambda & \cos L \\ -\sin \lambda & \cos \lambda & 0 \\ -\cos L \cos \lambda & \cos L \sin \lambda & -\sin L \end{bmatrix} \tag{31}$$

where  $L$  and  $\lambda$  are latitude and longitude, respectively.

The skew symmetry matrix related to the misalignment angle vector estimated in  $e$  frame is expressed in Equation (32).

$$\mathbf{C}_b^e \tilde{\mathbf{C}}_e^b = \mathbf{I} + (\boldsymbol{\phi}^e \times) = \begin{bmatrix} 1 & -\phi_z^e & \phi_y^e \\ \phi_z^e & 1 & -\phi_x^e \\ -\phi_y^e & \phi_x^e & 1 \end{bmatrix} \tag{32}$$

where  $\phi_x^e, \phi_y^e, \phi_z^e$  are the small misalignment angles represented in  $e$  frame.

Similarly, the skew symmetry matrix related to the misalignment angle vector estimated in  $n$  frame is expressed in Equation (33) as

$$\mathbf{C}_b^n \tilde{\mathbf{C}}_n^b = \begin{bmatrix} 1 & -\phi_D & \phi_E \\ \phi_D & 1 & -\phi_N \\ -\phi_E & \phi_N & 1 \end{bmatrix} \tag{33}$$

where  $\phi_N, \phi_E, \phi_D$  are the small misalignment angles represented in  $n$  frame.

Then the following equation can be formed from Equations (32) and (33)

$$\begin{aligned}
 \mathbf{C}_b^e \tilde{\mathbf{C}}_e^b &= \mathbf{C}_n^e \mathbf{C}_b^n \tilde{\mathbf{C}}_n^b \tilde{\mathbf{C}}_e^n \\
 &\approx \begin{bmatrix} -\sin L \cos \lambda & -\sin \lambda & -\cos L \cos \lambda \\ -\sin L \sin \lambda & \cos \lambda & \cos L \sin \lambda \\ \cos L & 0 & -\sin L \end{bmatrix} \begin{bmatrix} 1 & -\phi_D & \phi_E \\ \phi_D & 1 & -\phi_N \\ -\phi_E & \phi_N & 1 \end{bmatrix} \\
 &\times \begin{bmatrix} -\sin L \cos \lambda & -\sin L \sin \lambda & \cos L \\ -\sin \lambda & \cos \lambda & 0 \\ -\cos L \cos \lambda & \cos L \sin \lambda & -\sin L \end{bmatrix} \\
 &= \begin{bmatrix} 1 & -\phi_z^e & \phi_y^e \\ \phi_z^e & 1 & -\phi_x^e \\ -\phi_y^e & \phi_x^e & 1 \end{bmatrix}
 \end{aligned} \tag{34}$$

Ignoring the horizontal misalignment angles, Equation (34) can be written as

$$\begin{aligned}
 \begin{bmatrix} 1 & -\phi_D & 0 \\ \phi_D & 1 & 0 \\ 0 & 0 & 1 \end{bmatrix} &= \begin{bmatrix} -\sin L \cos \lambda & -\sin L \sin \lambda & \cos L \\ -\sin \lambda & \cos \lambda & 0 \\ -\cos L \cos \lambda & \cos L \sin \lambda & -\sin L \end{bmatrix} \\
 &\times \begin{bmatrix} 1 & -\phi_z^e & \phi_y^e \\ \phi_z^e & 1 & -\phi_x^e \\ -\phi_y^e & \phi_x^e & 1 \end{bmatrix} \begin{bmatrix} -\sin L \cos \lambda & -\sin \lambda & -\cos L \cos \lambda \\ -\sin L \sin \lambda & \cos \lambda & \cos L \sin \lambda \\ \cos L & 0 & -\sin L \end{bmatrix}
 \end{aligned} \tag{35}$$

From Equation (35),  $\phi_D$  can be expressed as

$$\begin{aligned}
 \phi_D &= \begin{bmatrix} 1 & -\phi_z^e & \phi_y^e \\ -\sin \lambda & \cos \lambda & 0 \\ -\phi_y^e & \phi_x^e & 1 \end{bmatrix} \begin{bmatrix} -\sin L \cos \lambda \\ -\sin L \sin \lambda \\ \cos L \end{bmatrix} \\
 &= (-\cos \lambda \cos L)\phi_x^e + (-\sin \lambda \cos L)\phi_y^e + (-\sin L)\phi_z^e
 \end{aligned} \tag{36}$$

As a result, the measurement equation related to the heading angle is obtained

$$\delta z_\psi = \tilde{\psi}^n - \psi^n = -\phi_D = \mathbf{H}_\psi \boldsymbol{\phi}^e \tag{37}$$

where

$$\mathbf{H}_\psi = \begin{bmatrix} \cos \lambda \cos L & \sin \lambda \cos L & \sin L \end{bmatrix} \tag{38}$$

In a unified form, the measurement error  $\delta z$  is expressed as

$$\delta z = \mathbf{H} \mathbf{x}_{LG-EKF} + \mathbf{v} \tag{39}$$

where

$$\delta \mathbf{z} = \begin{bmatrix} \delta z_v \\ \delta z_r \\ \delta z_\psi \end{bmatrix}, \mathbf{v} = \begin{bmatrix} \mathbf{v}_{v,3 \times 1} \\ \mathbf{v}_{r,3 \times 1} \\ \mathbf{v}_{\psi,1 \times 1} \end{bmatrix}, \mathbf{H} = \begin{bmatrix} (\tilde{\mathbf{v}}_{ib}^e \times) & -\mathbf{I}_3 & \mathbf{0}_{3 \times 3} & \mathbf{0}_{3 \times 3} & \mathbf{0}_{3 \times 3} \\ (\tilde{\mathbf{r}}_{ib}^e \times) & \mathbf{0}_{3 \times 3} & -\mathbf{I}_3 & \mathbf{0}_{3 \times 3} & \mathbf{0}_{3 \times 3} \\ \mathbf{H}_\psi & & & \mathbf{0}_{12 \times 1} & \end{bmatrix} \tag{40}$$

Finally, the navigation parameters should be corrected according to Equation (41)

$$\begin{bmatrix} \mathbf{C}_b^e & \mathbf{v}_{ib}^e & \mathbf{r}_{ib}^e \\ \mathbf{0}_{1 \times 3} & 1 & 0 \\ \mathbf{0}_{1 \times 3} & 0 & 1 \end{bmatrix} = \begin{bmatrix} \exp(\boldsymbol{\phi}^e \wedge) & \mathbf{J} \boldsymbol{\rho}_v^e & \mathbf{J} \boldsymbol{\rho}_r^e \\ \mathbf{0}_{1 \times 3} & 1 & 0 \\ \mathbf{0}_{1 \times 3} & 0 & 1 \end{bmatrix} \begin{bmatrix} \tilde{\mathbf{C}}_b^e & \tilde{\mathbf{v}}_{ib}^e & \tilde{\mathbf{r}}_{ib}^e \\ \mathbf{0}_{1 \times 3} & 1 & 0 \\ \mathbf{0}_{1 \times 3} & 0 & 1 \end{bmatrix} \tag{41}$$



Figure 1. Sensor configurations of the land vehicle field test.

Table 1. Specifications of the STIM300-IMU.

	Gyroscope	Accelerometer
Frequency	200 Hz	200 Hz
Dynamic range	±400°/s	±10 g
Bias	−250°/h ~ +250°/h	−2.3 mg ~ +2.3 mg
Bias instability	0.5°/h	0.05mg
Random walk	0.15°/√h	0.07m/s/√h

And the attitude parameters of roll, pitch and yaw in  $n$  frame can be obtained from

$$C_b^n = C_e^n C_b^e \tag{42}$$

### 6. Land vehicle field test

The land vehicle field test was conducted to compare the performance of EKF, ST-EKF and LG-EKF (proposed). The experiment platform consists of a GPS signal receiver, a MEMS-IMU (MIMU, Stim-300), a magnetometer chip (HMC5983) and a fibre optic gyroscope IMU (FOG-IMU) as the main reference system. The update interval of the GPS is 1 s, with single point positioning accuracy of 0.1 m/s and 5 m for the velocity and the position respectively. The detailed sensor configurations are illustrated in Figure 1. The specifications of the Stim-300 MIMU and HMC5983 are shown in Table 1 and Table 2 respectively. The trajectory of this experiment is drawn on the Ovita map (red line in Figure 2).

The total time length of the test was 1,094 s. All the sensors were well calibrated before the experiment, thanks to the work of He et al. (2020). The magnetometer heading angle error is presented in Figure 3, with mean 0.074° and standard deviation 2.017°. The initial attitude of the vehicle was given by the magnetometer heading angle and accelerometer-based levelling, it being unnecessary to



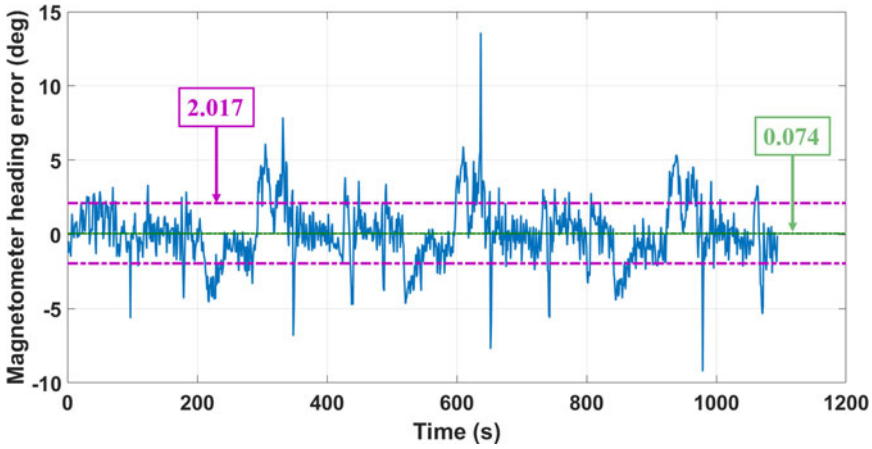


Figure 3. Heading error result of magnetometer in the land vehicle field test.

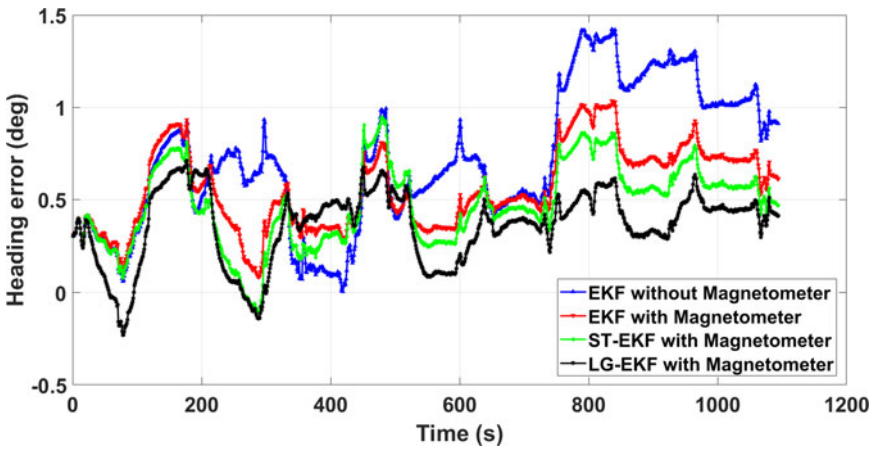


Figure 4. Heading error results in the land vehicle field test.

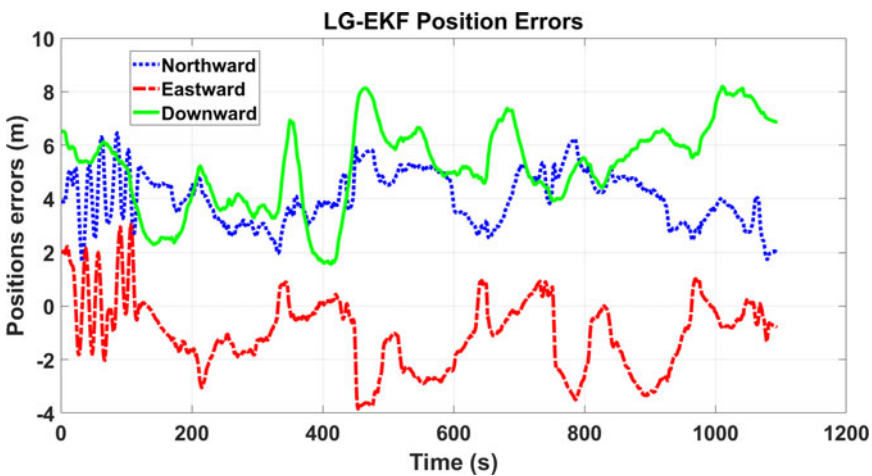
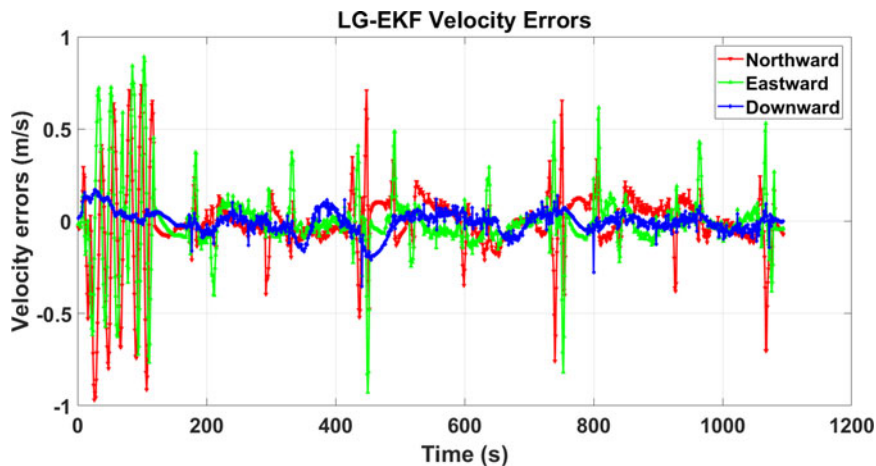


Figure 5. Position errors of LG-EKF in the land vehicle field test.



**Figure 6.** Velocity errors of LG-EKF in the land vehicle field test.

**Table 3.** Mean and RMS of the heading error results.

	Mean (deg)	RMS (deg)
EKF without magnetometer	0.7191	0.8064
EKF with magnetometer	0.5617	0.6036
ST-EKF with magnetometer	0.5196	0.4721
LG-EKF with magnetometer	0.3606	0.4104

**Table 4.** Mean and RMS of the roll error results.

	Mean (deg)	RMS (deg)
EKF without magnetometer	0.0095	0.0587
EKF with magnetometer	0.0145	0.0555
ST-EKF with magnetometer	0.0146	0.0552
LG-EKF with magnetometer	0.0053	0.0365

## 7. Conclusions

In this paper, an LG-EKF is proposed for the integrated navigation system to tackle the nonlinear problem. The SINS navigation differential equations in the ECEF frame are first derived, and then the novel nonlinear right-invariant state errors of SINS under the Lie group are defined, which are proved to be trajectory independent. The system equations of SINS are developed for the proposed nonlinear state errors. The specific force item is replaced by a gravitational related item in the new velocity differential equation, which improves robustness and accuracy of the navigation result. The corresponding measurement equations of velocity, position and heading angle for the proposed LG-EKF are derived. A land vehicle equipped with a MIMU/GPS/magnetometer system is used to conduct a field test, which validates that the GNSS/IMU integrated navigation system achieves a better attitude estimation with the assistance of a well-calibrated magnetometer. The proposed LG-EKF also has a better heading angle estimation accuracy compared with the traditional EKF and ST-EKF. The proposed LG-EKF with nonlinear state errors is not limited within this specific scenario but is capable of other navigation applications with various sensors, both high-end and low-end. To fully exploit the

**Table 5.** Mean and RMS of the pitch error results.

	Mean (deg)	RMS (deg)
EKF without magnetometer	0.0681	0.0876
EKF with magnetometer	0.0632	0.0834
ST-EKF with magnetometer	0.0626	0.0830
LG-EKF with magnetometer	0.0113	0.0113

potentialities of the LG-EKF, there remain many meaningful works could be done. The performance of the LG-EKF should be tested in more applications, for example, evaluating LG-EKF's accuracy and robustness in the integrated navigation assisted with other sensors, like odometer or atmospheric-pressure altimeter, and exploring the possibility of usage in visual-inertial odometry applications and so on.

### Funding statement

This work was supported by the Research Project of the National University of Defense Technology (grant number ZK19-26) and supported by the National Natural Science Foundation of China (No. 61573371, No. 61773394).

### References

- Andrie, M. S. and Crassidis, J. L. (2015). Attitude estimation employing common frame error representations. *Journal of Guidance Control and Dynamics*, **38**(9), 1614–1624.
- Barrau, A. and Bonnabel, S. (2017a). The invariant extended Kalman filter as a stable observer. *IEEE Transactions on Automatic Control*, **62**(4), 1797–1812.
- Barrau, A. and Bonnabel, S. (2017b). Three examples of the stability properties of the invariant extended Kalman filter. *IF AC-PapersOnLine*, **50**(1), 431–437.
- Barrau, A. and Bonnabel, S. (2020). Extended Kalman Filtering With Nonlinear Equality Constraints: A Geometric Approach. *IEEE Transactions on Automatic Control*, **65**(6), 2325–2338.
- Brossard, M., Bonnabel, S. and Barrau, A. (2018). Invariant Kalman filtering for visual inertial SLAM. *International Conference on Information Fusion*, 2021–2028.
- Brossard, M., Barrau, A. and Bonnabel, S. (2019). RINS-W: Robust Inertial Navigation System on Wheels. *2019 IEEE/RSJ International Conference on Intelligent Robots and Systems (IROS)*, 2068–2075.
- Cui, C., Zhao, J. and Hu, J. (2019). Improving robustness of the MAV yaw angle estimation for low-cost INS/GPS integration aided with tri-axial magnetometer calibrated by rotating the ellipsoid model. *IET Radar, Sonar & Navigation*, **14**(1), 61–70.
- Groves, P. D. (2013). *Principles of GNSS, Inertial, and Multisensor Integrated Navigation Systems*. London: Artech House.
- Hartley, R., Ghaffari, M. and Eustice, R. M. (2020). Contact-aided invariant extended Kalman filtering for robot state estimation. *The International Journal of Robotics Research*, **39**(4), 402–430.
- He, R., Hu, X., Zhang, L., He, X. and Han, G. (2020). A combination orientation compass based on the information of polarized skylight/geomagnetic/MIMU. *IEEE Access*, **8**, 10879–10887.
- Huang, G., Mourikis, A. I. and Roumeliotis, S. I. (2010). Observability-based rules for designing consistent EKF SLAM estimators. *The International Journal of Robotics Research*, **29**(5), 502–528.
- Jang, J. S. and Liccardo, D. (2007). Small UAV automation using MEMS. *IEEE Aerospace and Electronic Systems Magazine*, **22**(5), 30–34.
- Leclerc, J. (2007). MEMs for aerospace navigation. *IEEE Aerospace and Electronic Systems Magazine*, **22**(10), 31–36.
- Liang, H., Bai, H. and Liu, N. (2020). Polarized skylight compass based on a soft-margin support vector machine working in cloudy conditions. *Applied Optics*, **59**(5), 1271–1279.
- Miao, C., Cao, J. and Ou, Y. (2014). MEMS-SINS/GPS/magnetometer integrated navigation system for small unmanned aerial vehicles. *Applied Mechanics and Materials*, **568–570**, 976–986.
- Ravish, G., Jigyasha, M. and Pannaga, N. (2013). MEMS technology and application in defense navigation system. *International Journal of Engineering Research and Technology (IJERT)*, **2**(10), 1903–1909.
- Robert, E. and Perrot, T. (2017). Invariant Filtering Versus Other Robust Filtering Methods Applied to Integrated Navigation. *24th Saint Petersburg International Conference on Integrated Navigation Systems*, 1–7.
- Schmidt, S. F. (1966). Application of state-space methods to navigation problems. *Advances in Control Systems*, **3**, 293–340.

- Sebesta, K. D. and Boizot, N.** (2014). A real-time adaptive high-gain EKF, applied to a quadcopter inertial navigation system. *IEEE Transactions on Industrial Electronics*, **61**(1), 495–503.
- Wang, M., Wu, W., Zhou, P. and He, X.** (2018). State transformation extended Kalman filter for GPS/SINS tightly coupled integration. *GPS Solutions*, **22**(4), 1–12.
- Wang, M., Wu, W., He, X. and Pan, X.** (2019a). State Transformation Extended Kalman Filter for SINS Based Integrated Navigation System. *2019 DGON Inertial Sensors and Systems (ISS)*. IEEE.
- Wang, M., Wu, W., He, X. and Pan, X.** (2019b). Further explanation and application of state transformation extended Kalman filter. *Journal of Chinese Inertial Technology*, **27**(4), 500–509.
- Wang, M., Wu, W., He, X., Li, Y. and Pan, X.** (2019c). Consistent ST-EKF for long distance land vehicle navigation based on SINS/OD integration. *IEEE Transactions on Vehicular Technology*, **68**(11), 10525–10534.
- Wu, J.** (2019). Real-time magnetometer disturbance estimation via online nonlinear programming. *IEEE Sensors Journal*, **19**(12), 4405–4411.
- Wu, J., Liu, M., Huang, Y., Jin, C., Wu, Y. and Yu, C.** (2020). SE(n)++: An Efficient Solution to Multiple Pose Estimation Problems. *IEEE Transactions on Cybernetics*, 1–12.
- Wu, J., Zhou, Z., Chen, J., Fourati, H. and Li, R.** (2016). Fast complementary filter for attitude estimation using low-cost MARG sensors. *IEEE Sensors Journal*, **16**(18), 6997–7007.
- Wu, Y., Zou, D. and Liu, P.** (2018). Dynamic magnetometer calibration and alignment to inertial sensors by Kalman filtering. *IEEE Transactions on Control Systems and Technology*, **26**(2), 716–723.
- Xiang, X., Ming, L., Cao, G. and Xu, D.** (2019). Real-time calibration method for three-axis magnetometer based on adaptive parameter estimation. *Journal of Chinese Inertial Technology*, **27**(3), 384–389.